Langmuir

ARTICLE

pubs.acs.org/Langmuir

Assessment of Porosities of SBA-15 and MCM-41 Using Water Sorption Calorimetry

Vitaly Kocherbitov[†,*] and Viveka Alfredsson[‡]

[†]Biomedical Laboratory Science, Faculty of Health and Society, Malmö University, SE-205 06 Malmö, Sweden

[‡]Physical Chemistry, Center for Chemistry and Chemical Engineering, P.O. Box 124, Lund University, SE-221 00 Lund, Sweden

Supporting Information

ABSTRACT: Water sorption calorimetry has been used for characterization of 2D hexagonally ordered mesoporous silica SBA-15. Experimental data on water sorption isotherm, the enthalpy, and the entropy of hydration of SBA-15 are presented. The results were compared with previously published results on MCM-41 obtained using the same technique. The water sorption isotherm of SBA-15 consists of four regimes, while the sorption isotherm of MCM-41 consists only of three. The extra regime in the water sorption isotherm for SBA-15 arises from filling of intrawall pores, that are present in SBA-15 but absent in MCM-41. The water sorption isotherms of the two types of mesoporous silica were analyzed using the Barrett−Joyner−Halenda approach. For the BJH analysis, *t*-curves of silica with different degrees of hydroxylation were proposed. Comparison of water and nitrogen *t*-curves shows that, independent of hydroxylation of silica surface, the adsorbed film of water is much thinner than the adsorbed film of nitrogen at similar relative pressures. This fact decreases the uncertainty of the assessment of porosity with water sorption originated from variations in surface properties. The pore size distribution of SBA-15 calculated with BJH treatment of water sorption data is in good agreement with nitrogen NLDFT results on the same material.

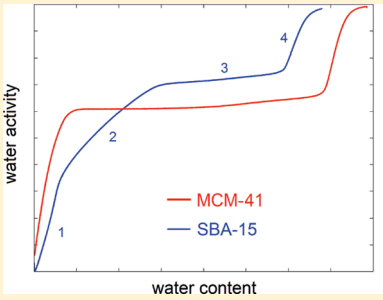

Intrawall pores induce an additional regime in the water sorption isotherm of SBA-15

INTRODUCTION

Ordered mesoporous silica materials are synthesized in a cooperative self-assembly process with a silica source and amphiphilic structure directors such as cationic surfactants or block copolymers. Removal of the amphiphiles by, for instance, calcination creates the porous structure. When surfactants with a compact hydrophilic headgroup are used in the synthesis (for example, alkyl trimethyl ammonium bromides in the synthesis of MCM-41), the resulting silica material contains only mesopores and their size distribution is rather narrow. However, when the substance used as a structure director has a hydrophilic headgroup that contains oligomeric chains of polyethylene oxide, the resulting silica material contains both mesopores and smaller intrawall pores[1] that can be either large micropores or small mesopores. In such materials (for example, SBA-15) the main mesopores are ordered in a 2D hexagonal pattern, while the intrawall pores on the other hand are disordered. Due to their disordered state, determination of their geometries is not trivial. For instance, as the intrawall pores are disordered, they do not give rise to Bragg peaks and therefore are not detectable in X-ray scattering experiments where the hexagonal pattern of mesopores in SBA-15 is clearly identified.

Combining X-ray scattering and nitrogen[2−4] or water[5] sorption measurements gives the most accurate data on pore sizes of hexagonally ordered materials like MCM-41. In this approach, the pore diameter is calculated using the X-ray data on the unit cell size and the sorption data on the volume fraction of mesopores. However, the nitrogen sorption data alone,[6] or as it was recently shown, water sorption data[5] can be used for reasonably accurate determinations of cylindrical pore sizes of MCM-41. Characterization of materials that contain two types of pores (such as SBA-15) is less straightforward. When nitrogen sorption is used, small pores are not seen in the sorption isotherm in the same way as the mesopores are seen, i.e., via the capillary condensation step/plateau. The capillary condensation of nitrogen in intrawall pores is masked by the adsorption of nitrogen on the walls of silica and these two processes cannot be easily distinguished. One way to obtain data on microporosity of SBA-15 is to use so-called *t*-plot, α_s-plot, and β_s-plot methods.[1,7−9] In these type of methods, the amount of nitrogen adsorbed by a microporous material at a given pressure is compared with the amount of nitrogen adsorbed by a reference material that does not have micropores.[10] Another way is to use nonlocal density functional theory (NLDFT) to treat nitrogen sorption data.[11,12] Also, a method of assessment of microporosity based on the variation of the parameter *C* of the BET equation was proposed.[13] These methods allow characterization of microporosity using nitrogen sorption data, although a common

Received: September 22, 2010
Revised: February 3, 2011
Published: March 02, 2011

disadvantage of these methods is that the presence of smaller pores is seen only from numerical evaluation of the data and not seen from the shape of the nitrogen sorption isotherms.

Adsorption of water vapor in porous materials features the same phenomena as the adsorption of nitrogen. At low pressures, molecules of water, in the same way as molecules of nitrogen, adsorb at the surface of a porous material; at higher pressures, capillary condensation is observed. An important difference between the processes of sorption of water and of nitrogen is in the amount of the adsorbate taken up by the porous substance before the capillary condensation begins. In a study of a mesoporous material MCM-41, we showed that the amount of water adsorbed by this material can be an order of magnitude lower than the amount of nitrogen adsorbed by the same material prior to capillary condensation.[5] The thickness of the preadsorbed layer of water is thus much smaller than the thickness of the preadsorbed layer of nitrogen. This implies that the smaller pores are easily filled with nitrogen without capillary condensation. They are therefore not directly manifested in the nitrogen sorption isotherm but can be observable in the water sorption isotherm.

As in any capillary condensation process, condensation of water in mesoporous silica may be accompanied by sorption−desorption hysteresis. It is, however, not clear whether physical hysteresis (resulting from change of meniscus type in sorption and desorption processes) takes place in the case of capillary condensation of water in mesoporous silica. To the best of our knowledge, the lower hysteresis closure point for water was never reported, while for nitrogen, it is known to be 0.42.[14] A hysteresis resulting from chemical modification of the silica surface by water (hydroxylation) does, however, take place. This is usually considered a disadvantage of the water sorption compared to nitrogen sorption. On the other hand, comparison of enthalpies of hydration of hydroxylated and nonhydroxylated mesoporous silica shows that a strong heat effect associated with chemical modification of the surface is not observed during adsorption and capillary condensation of water in nonhydroxylated silica.[5] This indicates that the chemical modification occurs at water activities higher than those needed for capillary condensation and therefore has little influence on the use of water adsorption for assessment of porosity. Moreover, comparison of the "first scan" and the "second scan" in water sorption experiments gives additional information about chemical properties of the studied surface.[5] Such information cannot be obtained from nitrogen sorption experiments.

Another advantage of the water sorption methods compared to nitrogen sorption is that the temperature of the sorption experiment is close to the temperatures normally required by practical applications of mesoporus materials, especially biomedical applications. While the temperature of a nitrogen sorption experiment is 77 K, the temperatures of water sorption experiments can vary in a relatively wide range typical for biological systems (for sorption calorimetric experiments it is usually from +15 °C to +75 °C). For pure silica, this may not be crucial, but for systems that include biomolecules (for example, proteins or lipids adsorbed in the porous structure) the temperature of the experiment can be an important parameter to control.

Here, we show that by using water sorption calorimetry one can directly determine the presence of smaller pores in hexagonally ordered silica materials like SBA-15 simply from the shape of the water sorption isotherms. Nitrogen sorption on the other hand, as mentioned above, requires numerical evaluation of the data and direct observation from the isotherms does not reveal the presence of micropores. The pore size distributions calculated from the water sorption isotherms using the BJH method are in good agreement with nitrogen NLDFT results. In addition to information on pore sizes, water sorption calorimetry provides experimental data on thermodynamics of water adsorption and capillary condensation.

EXPERIMENTAL SECTION

Synthesis. SBA-15 was synthesized according to a protocol originally based on the seminal SBA-15 paper[15] but slightly modified.[16] Tetramethyl orthosilicate (TMOS) was used as silica source and as structure director Pluronic P104 was used. This is a polyethylene oxide-polypropylene oxide-polyethylene oxide (EO_{27}-PO_{61}-EO_{27}) polymer. The following reagents and amounts were used: P104/0.48 g, 4 M HCl/7.5 g, H_2O (Millipore)/11.25 g, MeOH/0.152 g, and TMOS/0.715 mL. This makes a 2.5 wt % Pluronic solution in 1.6 M HCl. To this solution, held at 55 °C, TMOS was added and the resulting solution was stirred at this temperature for 24 h after which the solution was hydrothermally treated at 80 °C for 24 h. The silica powder was washed with water and then calcined at 500 °C for 6 h in order to remove the amphiphilic structure promoter. The obtained SBA-15 sample had a surface area of 738 m^2/g and a pore volume of 0.68 cm^3/g (measured using NLDFT method).

Calorimetry. Sorption calorimetric experiments were conducted at 25 °C in a two-chamber sorption calorimetric cell inserted in a double-twin microcalorimeter.[17] The SBA-15 sample was placed in the upper chamber, while pure water was injected in the lower chamber. In a sorption experiment, water evaporates from the lower chamber, diffuses through the tube that connects the two chambers, and is adsorbed by the sample in the upper chamber. The thermal powers released in the two chambers are monitored simultaneously. The activity of water a_w (the partial pressure of water in the sample divided by the partial pressure of water over the pure liquid water) in the sorption experiments was calculated from the thermal power of vaporization of water in the lower chamber as described previously.[18] Sorption isotherms of two nonhydroxylated SBA-15 samples with dry masses of 48.93 mg and 32.24 mg were measured. The obtained results were in good agreement with each other: the water activity values differed by less than 0.01 in almost the whole range of measured activities (both sorption isotherms are shown in Supporting Information).The partial molar enthalpy of mixing of water was calculated using the following equation:

$$H_w^{mix} = H_w^{vap} + H_w^{vap}\frac{P^{sorp}}{P^{vap}} \quad (1)$$

where P^{vap} and P^{sorp} are thermal powers registered in the vaporization and sorption chambers, respectively, and H_w^{vap} is the molar enthalpy of evaporation of pure water. The enthalpy of mixing considered here corresponds to the following reaction: $H_2O(l) \rightarrow H_2O(silica)$. For accurate calculation of the partial molar enthalpy of mixing of water, the sorption calorimeter was calibrated using magnesium nitrate as a standard substance.[19] The partial molar entropy of mixing of water was calculated from the enthalpy and the water activity data as follows:

$$S_w^{mix} = \frac{H_w^{mix}}{T} - R \ln a_w \quad (2)$$

where T is the absolute temperature, and R is the gas constant.

The desorption calorimetric experiments were done according to the method described in ref 20. In these experiments, magnesium nitrate solution was used to absorb water vapor released from samples obtained by mixing of dry SBA-15 with a certain amount of water.

Nitrogen Sorption. Nitrogen adsorption/desorption isotherms at 77 K were recorded using a Micromeritics ASAP 2400 instrument. The

pore size distributions were calculated from the adsorption and desorption branches of the N_2 sorption isotherm using the NLDFT method.[11,12]

RESULTS AND DISCUSSION

Results. The sorption isotherm of SBA-15 (water activity as function of water to silica mass ratio h_w) is shown in Figure 1. For comparison, the sorption isotherm of MCM-41 determined in our previous work[5] is also shown. The same sorption isotherms are also shown in Supporting Information as functions of water activity. There is a clear difference between the shapes of the SBA-15 and the MCM-41 sorption isotherms. The sorption isotherm of MCM-41 consists of three regimes: initial surface adsorption, capillary condensation, and post-capillary condensation uptake of water. In contrast, the sorption isotherm of SBA-15 consists of four pronounced regimes (Table 1). The additional regime spans form 0.06 to 0.295 g/g and can be attributed to capillary condensation of water in intrawall pores of SBA-15.

We also performed sorption experiments with SBA-15 samples synthesized at slightly different conditions (such as different temperatures and additions of alcohol; some examples are shown in Supporting Information) as well as with MCM-41 samples subjected to a postcalcination treatment with high humidity. In all cases, sorption isotherms of MCM-41 had only three regimes, while the sorption isotherms of SBA-15 always had four. This indicates that the additional regime is not caused by, e.g., differences in surface properties of the silica materials, but by the presence of the capillary condensation in the intrawall pores of SBA-15 that are absent in MCM-41.

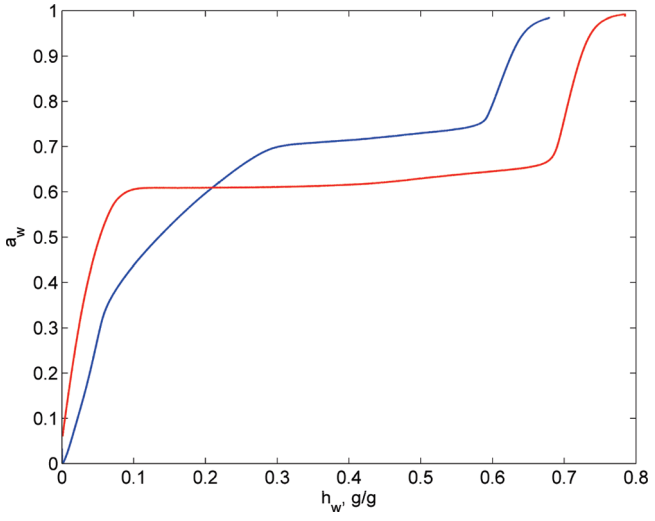

Figure 1. Water sorption isotherms of SBA-15 (blue curve) and MCM-41 (red curve). Water content is in mass of water per mass of dry silica.

The sorption calorimetry and other water sorption methods hence open new possibilities for characterization of micro- and mesoporosity of materials that contain more than one type of pore. At present, the microporosity of such materials is most often characterized by sorption of nitrogen at low temperatures. Nitrogen sorption isotherms of materials like SBA-15, however, consist only of three regimes (Figure 2), i.e., the adsorption and the capillary condensation of nitrogen in intrawall pores cannot be distinguished. Therefore, in order to determine the presence of intrawall pores using nitrogen sorption, one needs to use mathematical methods such *t*-plots, α_s-plots, or NLDFT. In the case of water, the formation of multilayers on the surface of silica is not as pronounced as in the nitrogen case. This can be seen from Figure 2: the amount of water adsorbed by SBA-15 at relative pressure of 0.1 is an order of magnitude lower than the amount of nitrogen adsorbed at the same relative pressure. This amount of water is not sufficient for filling the intrawall pores; therefore, adsorption and intrawall pore-filling can be clearly distinguished. Figure 1 shows that the presence of the intrawall pores can be seen simply from the shape of the sorption isotherm. The additional regime between adsorption and capillary condensation in the mesopores manifests the filling of the intrawall pores.

An additional advantage of water sorption calorimetry is the ability to measure not only the sorption isotherm, but also the enthalpy of hydration. Moreover, a combination of the two sets of data provides the means for calculating the entropy of hydration (the partial molar entropy of mixing of water S_w^{mix}). Both H_w^{mix} and S_w^{mix} are shown in Figure 3. In almost the whole range of water contents, the enthalpy and entropy effects have negative values; in other words, hydration is driven by enthalpy. The enthalpy and entropy curves can also be divided into four regimes that are in good correlation with the regimes determined from water sorption isotherm. The characteristics of those regimes are explained below.

Regimes of Sorption. *Regime 1.* In the beginning of sorption (at low water contents), the driving force of hydration is adsorption of water molecules to OH-groups of the silica surface. The most energetically favorable sorption sites are hydrated first and provide the strongest exothermic heat effect (about −13 kJ/mol). Then, weaker sorption sites are hydrated and the heat effect becomes weaker, i.e., less negative. Interestingly, the entropy of hydration goes through a minimum at a water content of about 0.02 g/g, while the enthalpy increases monotonously in the whole range of regime 1, prior to capillary condensation in micropores (regime 2). The minimum in entropy may be due to a more pronounced adsorption of water on preadsorbed molecules starting around the point of 0.02 g/g. When water starts to adsorb on top of other water molecules, this increases the

Table 1. Regimes of Water Sorption in SBA-15

regime	concentration range, h_w g/g	V_i, cm^3/g (SiO_2)	main processes
1	0.00−0.06	0.06[a]	adsorption in micro and mesopores
2	0.06−0.295	0.235	capillary condensation in intrawall pores, adsorption in mesopores
3	0.295−0.588	0.293	capillary condensation in mesopores
4	0.588−	-	further uptake of water

[a] For simplicity, the density of liquid water was assumed to be 1.0 cm^3/g

dx.doi.org/10.1021/la103807v |*Langmuir* 2011, 27, 3889–3897

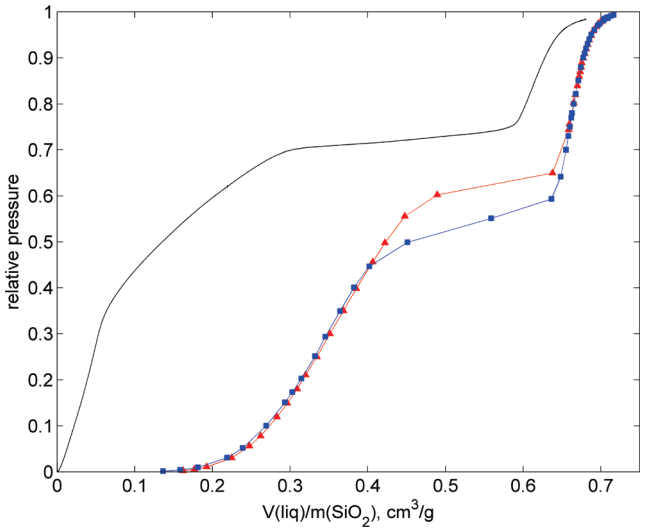

Figure 2. Comparison of water and nitrogen sorption isotherms of SBA-15. The amounts of nitrogen and water are expressed as volumes of the liquids per mass of silica. The solid curve denotes water sorption, red triangles denote nitrogen adsorption, and blue squares denote nitrogen desorption.

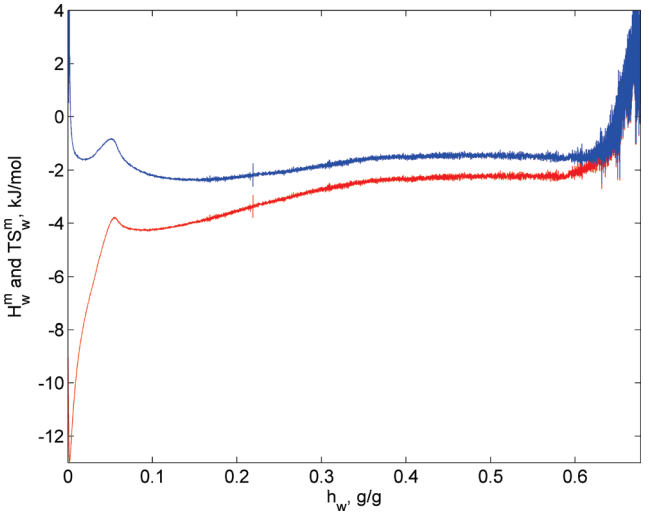

Figure 3. Partial molar enthalpy of mixing of water (red curve) and the partial molar entropy of mixing of water multiplied by temperature (blue curve) as functions of water content in SBA-15.

number of available sorption sites and the entropic effect becomes less negative.

Regime 2. This regime corresponds to capillary condensation of water in intrawall pores (large micropores and small mesopores) of SBA-15. Usually, for example in experiments with nitrogen sorption at 77 K, it is assumed that capillary condensation does not occur in micropores. In the present case, however, the situation is different. First, the micropores of SBA-15 are relatively large: about 2 nm (see discussion below). Since the diameter of a water molecule can be approximated as 0.3 nm, the cross-section of a micropore of SBA-15 is about 50 times larger than that of a water molecule, which provides plenty of room for capillary condensation of water (Figure 4). Second, the formation of multilayers of water on silica is much less pronounced

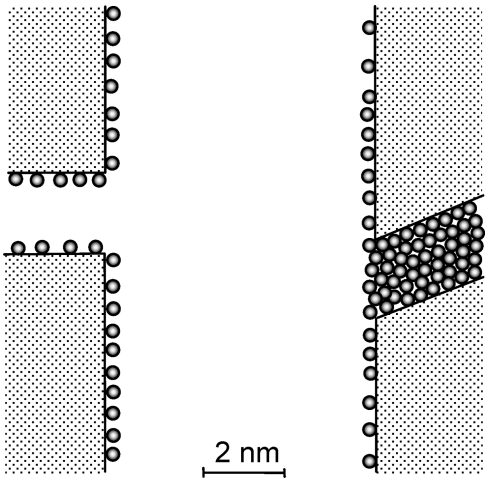

Figure 4. Schematic presentation of meso- and micropore sizes in SBA-15. Spheres of 0.3 nm diameter represent water molecules. The scheme corresponds to the 2nd regime of water sorption, where some micropores are filled with water and some are not.

than the formation of multilayers of nitrogen (clear evidence for this is presented in Figure 1 in ref 5). Thus, during initial sorption, water forms only thin layers on the silica surface and the bulk volume of the intrawall pores is filled during capillary condensation. Above a concentration of 0.06 g/g where the capillary condensation in micropores begins, both H_w^{mix} and S_w^{mix} become more negative. The main part of this effect arises from saturation of "dangling" (unsaturated) hydrogen bonds of preadsorbed water molecules: formation of the hydrogen bonds is an exothermic process and it also leads to orientational ordering of the "dangling" bonds when they become saturated. The value of the partial molar enthalpy of mixing H_w^{mix} in the second regime is close to that in the third regime (where the capillary condensation of water in mesopores occurs) and differs from that in the first regime (where adsorption of water molecules on silica walls is the main effect). This indicates that the nature of the intrawall pore filling (regime 2) is similar to capillary condensation of water in mesopores (regime 3). Both enthalpy and entropy effects become less pronounced during further water uptake, which reflects polydispersity of diameters and lengths of intrawall pores.

Regime 3. During capillary condensation in the mesopores, the enthalpy, entropy, and water activity curves level off, reflecting relatively monodisperse size distribution of the mesopores. The heat effect in this regime is less exothermic than in the regime 2 because the fraction of surface water molecules in mesopores is lower than that in the intrawall pores. On the molecular level, the exothermic heat effect arises from saturation of dangling hydrogen bonds of water molecules. Some of those water molecules are preadsorbed on silica walls during regimes 1 and 2; other molecules are on the surface of water that fills the intrawall pores that have openings to the mesopores (see the right part of Figure 4).

Regime 4. After capillary condensation, further uptake of water is accompanied by a sharp increase of enthalpy and entropy effects. This indicates disordering of the water structure in the pores upon increase of formal density of water in the pores. A similar effect was observed for the hydration of MCM-41.[5] Since the silica surface is not completely hydrophilic and contains small

dx.doi.org/10.1021/la103807v |*Langmuir* 2011, 27, 3889–3897

hydrophobic patches, unfilled cavities[21] can be formed during capillary condensation of water. In regime 4, the small unfilled cavities adjacent to hydrophobic patches are gradually filled with water, which leads to disruption of hydrogen bonds.

BJH Method. The water sorption isotherms presented in Figure 1 can be used to calculate the pore size distributions (PSD) in MCM-41 and SBA-15. One of the most common tools for calculations of pore size distributions in the case of nitrogen sorption is the Barrett−Joyner−Halenda (BJH) equation.[22] Its formal derivation is based on consideration of the desorption process (emptying the pores), but it works equally well for both sorption and desorption processes (if a hysteresis is not observed). According to the BJH equation, the volume V_{pn} of the pore emptied on n-th desorption step is calculated as follows:

$$V_{pn} = R_n \Delta V_n - R_n \Delta t_n \sum_{j=1}^{n-1} c_j A_{pj} \quad (3)$$

where parameters R_n and c are defined as

$$R_n = \left(\frac{\bar{r}_{pn}}{\bar{r}_{kn} + \Delta t_n} \right)^2 \quad (4)$$

and

$$c = \frac{\bar{r}_p - t_{\bar{r}}}{\bar{r}_p} \quad (5)$$

In eqs 3−5, ΔV_n is the volume of liquid desorbed in the n-th desorption step, Δt_n is the change of the thickness of the adsorbed layer, A_p is the area of the pore, r_{pn} and r_{kn} are the radii of the pore and of the evaporated "core" in the same step. For every desorption step n, the sum of cA_p for all previous steps is calculated (eq 3). The bar symbol means that the variable has the mean value between the beginning and the end of the desorption step.

The radius of the evaporated core of the cylindrical pore can be calculated from the Kelvin−Cohan equation:[23]

$$r_k = -\frac{2\gamma \cos\theta \cdot V_m}{RT \ln a_w} \quad (6)$$

where R is the gas constant, T is the temperature, γ is the surface tension (72 mJ/m^2 for water), θ is the contact angle of the surface, and V_m is the molar volume of liquid.

The only parameter in the set of equations shown above that in general cannot be directly calculated from the sorption isotherm is the thickness of the adsorbed layer t.

***t*-Curves for Water on Mesoporous Silica Surfaces.** A dependence of the statistical thickness of the adsorbed film t on the relative pressure is usually called a "t-curve". The thickness should be measured on a flat surface that does not have micropores. t-Curves are used to assess porosity and microporosity using sorption isotherms. For nitrogen, t-curves are well-established and routinely used in BJH method for calculations of pose size distributions of porous materials. Often, for practical purposes the nitrogen t-curve (in Å) is calculated from the following formula:[24]

$$t = \sqrt{\frac{13.99}{0.034 - \ln(p/p^0)}} \quad (7)$$

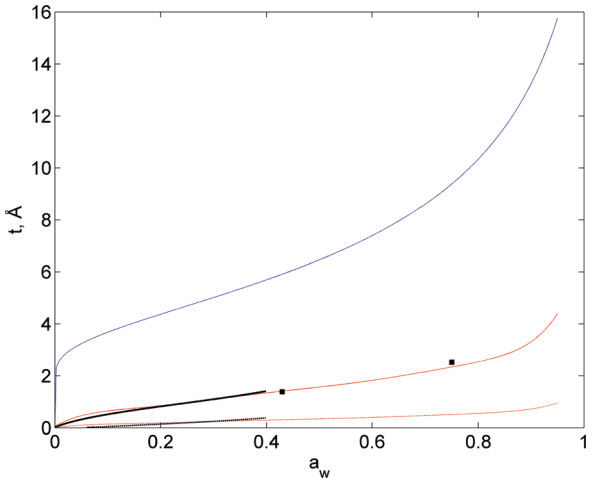

Figure 5. The nitrogen t-curve (blue curve), the water t-curves for MCM-41 (black curves), and the water t-curves calculated by scaling data of Hagymassy et al.[27] (red curves). The water t-curves for hydroxylated silica are shown as solid curves, for calcined silica as dotted curves. The squares show the thicknesses calculated from data of Collins et al.[28]

which is based on Harkins−Jura equation[25] assuming that the thickness t is proportional to the adsorbed volume V

$$t = \frac{V}{A} \quad (8)$$

The t-curve for nitrogen calculated using eq 7 is shown in Figure 5.

t-Curves for water are not as well established as those for nitrogen. The reason for this lies in the fact that water is more sensitive to properties of the surface than nitrogen is and hence the adsorbed layer thickness is dependent on the properties of the material. Ideally, for every type of a surface, a separate t-curve should be determined (in fact, this is strongly recommended not only for water, but also for other gases used for characterization of porosity[10,26]). For mesoporous silica, such curves may be determined based on water sorption isotherms of materials that do not have micropores, for example, MCM-41. On the basis of this method, the t-curves can be determined only at humidities that are lower than required for capillary condensation in mesopores. On the basis of water sorption isotherms of calcined and hydroxylated MCM-41,[5] we calculated t-curves for these types of mesoporous silica at water activities up to 0.4 (Figure 5). The surface areas used in the calculations were 994 and 942 m^2/g respectively. As expected, the thickness of the water film is larger in the case of the hydroxylated material compared to the calcined material. Nonetheless, both water t-curves lie much below the nitrogen t-curve, i.e., the thickness of the adsorbed water film is much smaller than the thickness of the adsorbed nitrogen film at similar relative pressures. Such a striking difference between adsorbed amounts of nitrogen and water on a silica surface shows that water, as an adsorptive, has not only limitations compared to nitrogen (higher sensitivity to the surface), but also certain clear advantages. Indeed, for determination of pore size distribution one needs to correct the amount of adsorptive that is released from the system upon decrease of pressure by the amount of adsorptive released due to the thinning of the adsorbed layer (the last term in eq 3). Obviously, the correction is smaller when the thickness of the adsorbed layer is smaller, which improves the

accuracy of calculations (provided that an adequate *t*-curve is selected).

For practical purposes of calculation of PSD in SBA-15, the water *t*-curves presented in Figure 5 as black curves cannot be used because they do not cover the range of water activities needed for characterization of SBA-15. Therefore, in our calculations we used an approach (described below) based on scaling the data on the number of multilayers of water with a statistical thickness of a multilayer calculated from the MCM-41 isotherms.

One of the first *t*-curves for water was proposed by Hagymassy, Brunauer, and Mikhail[27] who analyzed eleven water sorption isotherms of different materials. However, they did not present the data as water film thickness as a function of relative humidity, but as the number of layers as function of the relative humidity and suggested that the thickness should be calculated by multiplying the number of layers by the statistical thickness of a monolayer. As we showed earlier,[5] the monolayer of water on the surface of mesoporous silica should be viewed as a discontinuous layer where the whole surface is not covered by water molecules due to incomplete hydroxylation of the silica surface. One should note that this view of a monolayer agrees with IUPAC recommendations[26] that state that a monolayer of molecules may adopt a different structure than a close-packed array. In this case, the statistical thickness of this monolayer calculated using eq 8 will be lower than the size of a water molecule. Since water is sensitive to the properties of solids, an effective statistical thickness of a monolayer should be calculated separately for different surfaces.

According to Hagymassy et al.,[27] the monolayer thickness is achieved at a water activity about 0.3. Therefore, in order to calculate water *t*-curves for freshly calcined and hydroxylated silica materials, we multiplied the number of layers by the statistical thicknesses of monolayers of the two types of silica at water activity 0.3 (0.24 Å and 1.1 Å, respectively). The resulting *t*-curves are shown in Figure 5. The *t*-curve for hydroxylated silica is in good agreement with the thicknesses calculated from the data of Collins et al.[28] on hydroxylated silicas which lends further credibility to the approach used.

In practice, properties of many silica materials are in between these two extremes: freshly calcined and hydroxylated silica. Often, calcined materials are stored for a significant time, and during the storage, they slowly become more hydrophilic. The SBA-15 silica used here was also stored for some time prior to the calorimetric experiments and therefore cannot be considered as freshly calcined. In the following part of the article, this type of samples will be referred to as "stored". To determine the thickness of the water film adsorbed on the stored SBA-15 at 30% RH, we divided the adsorbed amount (0.053 g/g) by the BET surface area of SBA-15 (738 m^2/g). The result is 0.72 Å, and in agreement with expectations, it falls in between the values obtained for the other two types of silica (see Table 2).

Calculation of the pore size distribution requires information on the contact angle of the surface. For hydroxylated surfaces, zero is a good approximation, for freshly calcined mesoporous silica the value of 34° can be used.[5] The contact angle of stored silica can be estimated by the equation proposed by Lamb and Furlong:[29]

$$\cos\theta = 0.257 \cdot a(\mathrm{SiOH}) + 0.743 \qquad (9)$$

where $a(\mathrm{SiOH})$ is the fraction of silanol groups on the surface. We also used this equation in our previous work[5] to determine the contact angle of calcined MCM-41. The values of contact angles of the three types of silica are shown in Table 2.

Table 2. Recommended Parameters for Calculation of Pores Size Distribution

type of silica	*t*, Å at 30% RH	contact angle, deg
freshly calcined	0.24	34
stored	0.72	28
hydroxylated	1.1	0

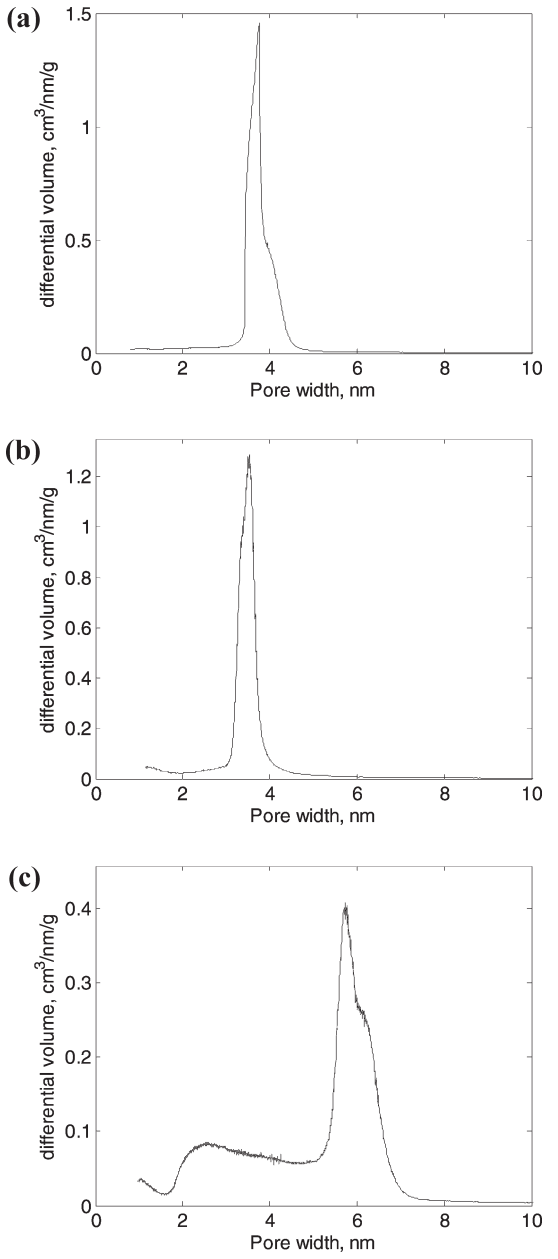

Figure 6. Pore size distributions of freshly calcined MCM-41 (a), hydroxylated MCM-41 (b), and stored SBA-15 (c) calculated from water sorption data.

Pore Size Distributions of MCM-41 and SBA-15. Pore size distributions of MCM-41 and SBA-15 calculated using eq 3 are

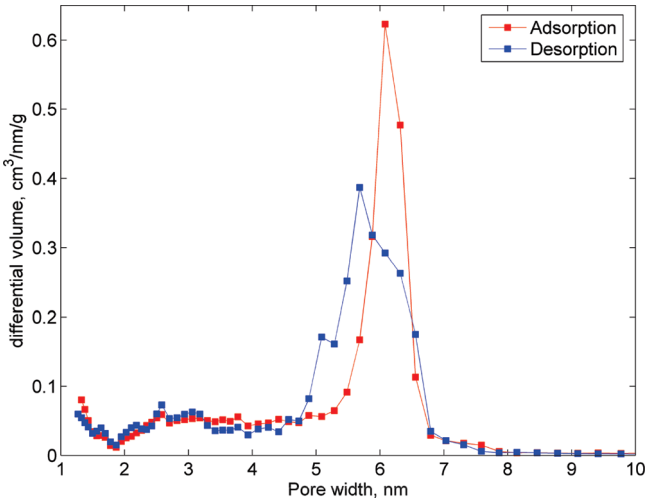

Figure 7. Pore size distribution calculated from nitrogen sorption data using NLDFT method.

shown in Figure 6. The PSD of freshly calcined MCM-41 has a shape of a sharp peak with a shoulder on its right side. The position of the peak maximum is in excellent agreement with the pore width calculated for the same sample using a combination of X-ray scattering data with sorption data.[5] The position of the maximum of PSD of hydroxylated MCM-41 is slightly shifted toward smaller widths. This shift arises from a decrease of the pore volume due to chemical modification of the surface with formation of silanol groups.

The pore size distribution of SBA-15 calculated from water sorption data is shown in Figure 6c. This PSD features not only the main peak that corresponds to main mesoporous channels of SBA-15, but also a substantial amount of pores in the range between 2 and 5 nm (intrawall pores). This pore size distribution is in good agreement with PSD obtained using NLDFT treatment of nitrogen sorption data on the same sample (Figure 7). Interestingly, even the shoulder on the right side of the main peak is seen in both water sorption and nitrogen desorption pore size distribution curves. The origin of this small shoulder in not completely clear, but most probably it reflects only the properties of this particular SBA-15 sample because this feature was not observed in other studies of SBA-15 (see, for example, ref 30). We should point out the fact that the PSD obtained from water adsorption is consistent with PSD obtained from nitrogen desorption (not nitrogen adsorption!). This indicates that the problem of metastability of adsorption branch (typically observed in case of nitrogen) was not present in the case of water adsorption in this particular sample. The fact that the PSDs obtained by the NLDFT model from the adsorption and the desorption branches of the nitrogen sorption do not coincide has previously been described to arise from the presence of intrawall pores (in the mesopore range), connecting the primary mesopores.[30] It should be noted that the SBA-15 in this work was synthesized with a block copolymer (P104) with longer (EO) chains than the ones normally used (P103 and P123). As the (EO)-chains give rise to the intrawall porosity (see below), longer chains are likely to give more intrawall porosity and are thereby a likely cause of the discrepancy in the PSD calculated for the desorption and adsorption branches of this particular SBA-15 material.

The parts of the PSD curves corresponding to intrawall pores have similar shapes both for nitrogen and for water showing a local maximum at about 2.5 nm in both cases.

The intrawall porosity in SBA-15 arises from the presence of polyethylene oxide chains in the silica wall that turn into small pores upon calcination. The length of the intrawall pores is limited (it is improbable that they go strictly in parallel with the main channels). This means that during the intrawall pore filling not only is the interface between the silica and gas removed but also an interface between liquid and gas is created at the ends of the intrawall pores (see Figure 4). This increases the relative pressure required for intrawall pore filling and therefore shifts the calculated pore sizes to higher values. This is the reason for obtained continuous distributions of the pore sizes from 2 to 5 nm, while most probably the intrawall pores have diameters close to the position of the local maximum of the distribution curves. This is however a common problem for both nitrogen and water sorption methodology which, to the best of our knowledge, does not have a straightforward solution.

Nonetheless, one can quantitatively estimate an effect of finite pore lengths on calculation of pore widths. In derivation of the Kelvin−Cohan equation (eq 6), it is assumed that the change of Gibbs energy has two contributions: a positive contribution from condensation of gas at pressures below saturation pressure and a negative contribution from the change of the type of interface. If the pore has a finite length L, then a third contribution comes about:

$$\Delta G = \frac{\pi r_k^2 L}{V_w} RT \ln \frac{p^0}{p} + 2\pi r_k L(\gamma_{SL} - \gamma_{SV}) + 2\pi r_k^2 \gamma_{LV} \quad (10)$$

Assuming an equilibrium process with zero change of Gibbs energy, we arrive at the following equation:

$$RT \ln a_w = -\frac{2\gamma \cos\theta \cdot V_w}{r_k} + \frac{2\gamma V_w}{L} \quad (11)$$

which is a generalization of the Kelvin−Cohan equation for finite pore lengths.

For illustration, we applied eq 11 to pores that correspond to the shallow minimum on pore size distribution curve of SBA-15 (see Figure 6c). Formally, the pore size at the minimum is 4.7 nm, although in reality, it is smaller due to finite pore length. Water activity at this point is 0.658; the minimum pore length of SBA-15 materials is about 3 nm.[11] The pore width calculated using eq 11 and corrected for the adsorbed layer of water is then 2.7 nm, which is close to the local maximum on the PSD curve. This illustrates that the left-hand part of the pore size distribution of SBA-15 reflects not only the distribution of widths of pores, but also distribution of their lengths. The real pore size distribution of SBA-15 may thus consist of two isolated peaks, one centered at about 2−3 nm and the other centered at about 6 nm.

Stability of the Method with Respect to Silica Surface Properties. Properties of the silica surface affect the adsorption behavior of water and other adsorptives. It is commonly agreed that in the case of water the effect of the chemistry of the surface is more pronounced than in case of nitrogen and we do not challenge this point of view. Indeed, unlike nitrogen, water is capable of forming hydrogen bonds with the surface which affects the thickness of the adsorbed film at given vapor pressure. However, as we showed above, the thickness of adsorbed water film is smaller than the thickness of an adsorbed nitrogen film at

similar pressures. Therefore, variations in the thicknesses of water films are variations of small values, while variations of thicknesses of nitrogen films are variations of large values. When the properties of the silica surface are known (Table 2), application of water sorption methods (such as sorption calorimetry) gives accurate results, as one can see from comparison of PSD obtained from water sorption (Figure 6 c) and from nitrogen NLDFT method (Figure 7) which is one of the most accurate methods of assessment of porosity.[14]

When the properties of the silica surface are not known, this can lead to an error of about 1 nm in assessment of diameters of pores using eq 3. To illustrate it, we calculated PSDs of SBA-15 using three different sets of parameters from Table 2. Using parameters recommended for freshly calcined, stored, and hydroxylated silica, we obtained maxima on the PSD curves at 5.2, 5.7, and 6.6 nm. This shows that, for accurate calculations using water sorption, the properties of silica should be known.

One should also note that water sorption isotherms themselves are sources of information on the surface properties, and in many cases, no additional information on the surface properties is needed. Indeed, one can calculate PSD using eq 3 with, for example, parameters for stored silica to get an estimate of surface area of the sample. Then, using eq 8 one can calculate the statistical thickness of monolayer and the contact angle using eq 9. The calculated parameters can be used to calculate PSD in a second iteration.

Sorption−Desorption Hysteresis. It is now agreed[14] that, in the case of the presence of physical sorption−desorption hysteresis, desorption but not adsorption branch represents equilibrium sorption process and therefore should be used for pore characterization. During adsorption when a cylindrical meniscus exists, the observed pressure may go higher than equilibrium level, while during desorption, a hemispherical meniscus corresponds to equilibrium conditions. In practice, the presence or absence of hysteresis depends on adsorbent and adsorbate type, temperature of the experiment, and the relative pressure level. For example, it is established that nitrogen sorption hysteresis does not exist at relative pressures below 0.42 at 77 K.[14,31] As a consequence, we did not find nitrogen sorption hysteresis in a MCM-41 sample[5] but observed it in SBA-15 sample, that has larger pores (see Figure 2). The limit for reversible capillary condensation for water is to the best of our knowledge not known. The reason for this is the presence of two types of hysteresis in water sorption experiments: chemical (due to surface modification) and physical (due to different types of meniscus). Therefore, the presence or absence of chemical or physical hysteresis should be established in the case of every sample studied by means of water sorption.

For the SBA-15 sample studied in this work, we investigated the presence of the sorption−desorption hysteresis using the method of desorption calorimetry.[20] Due to limitations of the method, the desorption experiments were done only down to water activity value of 0.675. More details about the experiment, as well as the partial desorption isotherm of SBA-15, are shown in the Supporting Information. The analysis of the desorption isotherm revealed a small hysteresis of about 0.036 units of water activity. In order to elucidate the nature of this hysteresis, we performed a calculation of a chemical hysteresis expected due to changes of the contact angle and the thickness of preadsorbed water layer. The result of the calculation (0.0353) is in excellent agreement with the experimentally observed value (more details are given in Supporting Information). This indicates that the hysteresis observed in the present case is of a chemical nature, and therefore, the physical hysteresis was not present in the conditions of the experiment. Hence, adsorption isotherm of SBA-15 can be used for calculations of pore size distribution. One should, however, note that this conclusion is valid only for the sample studied in the present work, and the presence or absence of physical hysteresis of water sorption should be established for each studied sample.

CONCLUSIONS

Water sorption can be used for comparison of mesoporous materials containing and not containing intrawall pores. The conclusions are as follows:

- In sorption isotherms of SBA-15, the presence of intrawall pores is seen as an additional regime of condensation of water in intrawall pores between the regimes of surface adsorption and capillary condensation in mesopores observed in MCM-41.
- Water sorption calorimetry provides information about the enthalpy and entropy of sorption, and for both materials (SBA-15 and MCM-41) in all regimes of sorption except for the last one, the enthalpy and the entropy of hydration are negative
- Water *t*-curves for mesoporous silica were constructed; the adsorbed film of water is much thinner than the adsorbed film of nitrogen at similar pressures.
- When the hydrophilicity/hydrophobicity of the silica surface is known (or can be estimated from the water sorption data), the water sorption isotherms can be used for calculation of pore size distribution.
- The pore size distribution of SBA-15 estimated from the water sorption data is in good agreement with nitrogen sorption NLDFT analysis.

ASSOCIATED CONTENT

Supporting Information. Water sorption isotherms presented as functions of relative pressure; water desorption isotherm; a *MATLAB* expression for generating water *t*-curves for three types of silica. This material is available free of charge via the Internet at http://pubs.acs.org.

AUTHOR INFORMATION

Corresponding Author

*Address: Faculty of Health and Society, Malmö University, SE-205 06 Malmö, Sweden. Ph: +4640 6657946. Fax: +4640 6658100. E-mail: Vitaly.Kocherbitov@mah.se.

ACKNOWLEDGMENT

We thank Peter Linton and Nina V. Reichhardt (Lund University) for synthesising the SBA-15 samples. John Landers and Alexander V. Neimark (Rutgers University) are acknowledged for calculation of the pore size distribution using NLDFT and the discussion of the results of the calculation respectively. Financial support from the Linnaeus Centre of Excellence Organizing Molecular Matter and from the Swedish Research Council (VA) is acknowledged.

REFERENCES

(1) Imperor-Clerc, M.; Davidson, P.; Davidson, A. *J. Am. Chem. Soc.* **2000**, *122* (48), 11925–11933.
(2) Kruk, M.; Jaroniec, M.; Sayari, A. *J. Phys. Chem. B* **1997**, *101* (4), 583–589.
(3) Dabadie, T.; Ayral, A.; Guizard, C.; Cot, L.; Lacan, P. *J. Mater. Chem.* **1996**, *6* (11), 1789–1794.
(4) Kruk, M.; Jaroniec, M.; Sakamoto, Y.; Terasaki, O.; Ryoo, R.; Ko, C. H. *J. Phys. Chem. B* **2000**, *104* (2), 292–301.
(5) Kocherbitov, V.; Alfredsson, V. *J. Phys. Chem. C.* **2007**, *111* (35), 12906–12913.
(6) Kruk, M.; Jaroniec, M.; Sayari, A. *Langmuir* **1997**, *13* (23), 6267–6273.
(7) Lukens, W. W.; Schmidt-Winkel, P.; Zhao, D. Y.; Feng, J. L.; Stucky, G. D. *Langmuir* **1999**, *15* (16), 5403–5409.
(8) Miyazawa, K.; Inagaki, S. *Chem. Commun* **2000**, *21*, 2121–2122.
(9) Ryoo, R.; Ko, C. H.; Kruk, M.; Antochshuk, V.; Jaroniec, M. *J. Phys. Chem. B* **2000**, *104* (48), 11465–11471.
(10) Rouquerol, F.; Rouquerol, J.; Sing, K. *Adsorption by powders and porous solids*; Academic Press: London, 1999.
(11) Ravikovitch, P. I.; Neimark, A. V. *J. Phys. Chem. B* **2001**, *105* (29), 6817–6823.
(12) Guillet-Nicolas, R.; Bérube, F.; Kim, T.-W.; Thommes, M.; Kleitz, F. Tailoring mesoporosity and intrawall porosity in large pore silicas: synthesis and nitrogen sorption behavior. In *Studies in Surface Science and Catalysis*, Gedeon, A., Massiani, P., Babonneau, F., Eds.; Paris, 2008; Vol. 174, pp 141−148.
(13) Knowles, J.; Armatas, G.; Hudson, M.; Pomonis, P. *Langmuir* **2006**, *22* (1), 410–418.
(14) Lowell, S.; Shields, J. E.; Thomas, M. A.; Thommes, M., *Characterization of Porous Solids and Powders: Surface Area, Pore Size and Density*.;Springer: Berlin, 2006; p 347.
(15) Zhao, D. Y.; Feng, J. L.; Huo, Q. S.; Melosh, N.; Fredrickson, G. H.; Chmelka, B. F.; Stucky, G. D. *Science* **1998**, *279* (5350), 548–552.
(16) Linton, P.; Alfredsson, V. *Chem. Mater.* **2008**, *20* (9), 2878–2880.
(17) Wadsö, L.; Markova, N. *Rev. Sci. Instrum.* **2002**, *73* (7), 2743–2754.
(18) Kocherbitov, V. *Thermochim. Acta* **2004**, *414* (1), 43–45.
(19) Kocherbitov, V. *Thermochim. Acta* **2004**, *421* (1−2), 105–110.
(20) Kocherbitov, V.; Wadsö, L. *Thermochim. Acta* **2004**, *411* (1), 31–36.
(21) Kocherbitov, V. *J. Phys. Chem. C* **2008**, *112* (43), 16893–16897.
(22) Barrett, E. P.; Joyner, L. G.; Halenda, P. P. *J. Am. Chem. Soc.* **1951**, *73*, 373–380.
(23) Cohan, L. H. *J. Am. Chem. Soc.* **1938**, *60* (2), 433–435.
(24) de Boer, J. H.; Lippens, B. C.; Linsen, B. G.; Broekhoff, J. C. P.; van der Heuvel, A.; Osinga, T. J. *J. Colloid Interface Sci.* **1966**, *21* (4), 405–414.
(25) Harkins, W.; Jura, G. *J. Am. Chem. Soc.* **1944**, *66* (8), 1366–1373.
(26) Sing, K. S. W.; Everett, D. H.; Haul, R. A. W.; Moscou, L.; Pierotti, R. A.; Rouquerol, J.; Siemieniewska, T. *Pure Appl. Chem.* **1985**, *57* (4), 603–619.
(27) Hagymassy, J.; Brunauer, S.; Mikhail, R. S. *J. Colloid Interface Sci.* **1969**, *29* (3), 485–491.
(28) Collins, K. E.; de Camargo, V. R.; Dimiras, A. B.; Menezes, D. T. C.; da Silva, P. A.; Collins, C. H. *J. Colloid Interface Sci.* **2005**, *291* (2), 353–360.
(29) Lamb, R. N.; Furlong, D. N. *J. Chem. Soc., Faraday Trans. 1* **1982**, *78* (1), 61–73.
(30) Kleitz, F.; Berube, F.; Guillet-Nicolas, R.; Yang, C. M.; Thommes, M. *J. Phys. Chem. C* **2010**, *114* (20), 9344–9355.
(31) Tompsett, G. A.; Krogh, L.; Griffin, D. W.; Conner, W. C. *Langmuir* **2005**, *21* (18), 8214–8225.